Applied Surface Science 448 (2018) 30–40

Contents lists available at ScienceDirect

Applied Surface Science

journal homepage: www.elsevier.com/locate/apsusc

Full Length Article

Characterization of the morphology, structure and wettability of phase dependent lamellar and nanotube oxides on anodized Ti-10Nb alloy

Aline R. Luz [a,*], Luciane S. Santos [b], Carlos M. Lepienski [a,c], Pedro B. Kuroda [d], Neide K. Kuromoto [a,e]

[a] Universidade Federal do Paraná, Programa de Pós-Graduação em Engenharia e Ciência dos Materiais – PIPE, 81.531-990 Curitiba, PR, Brazil
[b] Pontifícia Universidade Católica do Paraná, Escola Politécnica, Departamento de Engenharia Mecânica, 80.215 901 Curitiba, PR, Brazil
[c] Universidade Tecnológica Federal do Paraná, Programa de Pós-graduação em Engenharia Mecânica e de Materiais, 81.280-340 Curitiba, PR, Brazil
[d] Universidade Estadual Paulista, Laboratório de Anelasticidade e Biomateriais, Departamento de Física, 17.033-360 Bauru, SP, Brazil
[e] Universidade Federal do Paraná, Departamento de Física, 81.531-990 Curitiba, PR, Brazil

ARTICLE INFO

Article history:
Received 16 November 2017
Revised 15 March 2018
Accepted 8 April 2018
Available online 10 April 2018

Keywords:
Alpha–beta alloy
Ti-10Nb alloy
Nanotubes
Lamellar structure
Phosphorus incorporation
Wettability

ABSTRACT

Nanotubes grown on Ti and its alloys have been extensively investigated for the biomaterials applications, since these structures improve the surface biocompatibility and the corrosion resistance due to oxide formation. Some researchers showed that the microstructure of the pure Ti affect the morphology of nanotubes grown by anodic process. However, this subject is rarely investigated for nanotubes grown on Ti alloys. In the same way, nanostructured films formed by concomitant regions of tubes and lamellar structures hardly ever were reported. Investigations concerning these topics are required once beta titanium alloys are suitable candidates to replace the pure Ti and Ti-Al-V alloys for biomedical applications. Beta alloys composed of non-toxic elements (Nb, Ta, Mo) are biocompatible and have an excellent mechanical properties and corrosion resistance. The present work investigated questions regarding to the effect of microstructure of Ti-10Nb alloy on morphology of nanostructured film growth by anodization. The morphology, thickness, composition and atomic arrangement (amorphous/crystalline) of formed oxides, and the contact angle of anodic film were investigated. The X-ray diffraction patterns and SEM image show that the Ti-10Nb alloy is composed by alpha (hcp) and beta (bcc) phases. SEM and TEM techniques revel that self-organized nanotubes grew on alpha phase, whereas a lamellar structure with transversal holes grew on β-phase. Crystalline oxides are formed at oxide-metal interface, as indicated by X-ray diffraction patterns. However, the tubes and lamellas grown over the compact oxide are amorphous, as-prepared and annealed at 230 °C for 3 h, as showed by SAED patterns. The nanostructured films annealed at 430 °C and at 530 °C were damaged. A few changes were observed in XRD patterns of film annealed at 230 °C while the morphology held similar as the unannealed film. Finally, the presence of phosphorus ions incorporated into the anodic layer makes the surface hydrophilic, since a similar nanostructured film without phosphorous incorporation results hydrophobic.

1. Introduction

Titanium alloys are largely used to fabricate endosseous implants due to its higher biocompatibility when compared to other metals [1]. Although, there is a concernment about the long-term release of harmful ions, as aluminum and vanadium by dissolution from the Ti6Al4V alloy [1,2]. Those ions are associated with the development of neurological diseases, such as Alzheimer, and accumulation on kidneys and liver [3]. In order to overcome this drawback, many researchers propose the development of other biomedical titanium alloys, prioritizing the utilization of non-harmful elements and looking for the optimization of its mechanical properties [4]. Among these alloys, β-type TiNb alloys are being proposed as an alternative since those alloys have low elastic modulus, what could prevent the bone resorption caused by the mismatch between the bone and biomaterial elastic modulus [4,5].

Surface modifications in metallic implants improve the biological interaction since the early stage of contact. Surfaces tailored in nanoscale are known to improve the hydroxyapatite deposition [6]. Nanotube arrays can be easily obtained on titanium alloys by electrochemical techniques, such as anodic oxidation [7,8]. Nanotubes improve the osseointegration rate by increasing the surface wettability and modulating the cell response due to its morphology [9].

* Corresponding author.
E-mail addresses: alineluz@ufpr.br, arossettoluz@gmail.com (A.R. Luz), lepiensm@fisica.ufpr.br (C.M. Lepienski), kuromoto@fisica.ufpr.br (N.K. Kuromoto).

https://doi.org/10.1016/j.apsusc.2018.04.079
0169-4332/

Different factors and their influence on nanotubes have been investigated with details, such as pH, fluoride content, ageing of the electrolyte, anodizing potential and time, current density and temperature; which were summarized by several review [10]. Some authors investigated the effect of Ti crystalline orientation/microstructure on morphology nanotubes [11–17] and others for porous films obtained by anodic process [18–23].

For Ti alloys it is expected that the growth of films depends on the type of crystalline phase, number of phases and their surface distribution, as well as on the type and concentration of the constitutive elements [24,25]. However, few researchers make a consistent report about this subject for β-type alloys [24–28].

To obtain self-organized nanotubes can be used mixtures of the phosphoric acid plus fluorine ions, for example NH_4F, HF and NaF [29–32]. The success to grow nanotubes with these electrolytes can be attributed to fact that the phosphoric acid acts as a buffer species regulating the local acidification during pore growth [29]. The data of some researches showed that nanotubes grew in mixtures of the H_3PO_4 plus fluorine ions are hydrophilic surfaces [29,33,34]. In the same way, the presence of phosphorus ions into electrolyte improved the wettability of films obtained by plasma electrolytic oxidation [24,35,36].

However, comparing of wettability results it is not possible because the surface wettability depends on applied processing parameters [33]. And in doing so it is govern by the morphology, surface chemistry and free energy [37]. For nanotubes, it is well known that its morphology favors the liquid to penetrate into the tube, thus a lower the contact angle can be observed [37]. Likewise, the increase of nanotube diameter and/or its length decrease the contact angle, indicating an improve in surface wettability [37,38].

In this research, nanostructured films composed of nanotubes and lamellas were grown on Ti-10Nb alloy employing the electrolyte containing H_3PO_4 plus NH_4F. The objective was to analyze the morphology and the crystal structure of the different morphologies of film, i.e., nanotubes, lamellar structure and nanotubes plus lamellar structure of samples unannealed and annealed by TEM (Transmission Electron Microscopy) and SAED (Selected Area Electron Diffraction) techniques. It is the first time that analyses are reported for nanostructures of nanotubes and lamellas grown on a Ti alloy and the morphology varies according to substrate microstructure.

In addition, the wettability was investigated to determine its suitability to be used as a surface modification in Ti-10Nb implants. To discuss the wettability behavior due to the phosphorous incorporation into anodic film obtained in this work, the results were compared to additional wettability results of nanostructured films free of phosphorous incorporation reported elsewhere [26].

2. Materials and methods

Ti-10Nb alloy was prepared in the form of ingots from high purity Ti (99.7%) and Nb samples (99.98%). For the fusion of elements, it was used an arc melting furnace with cooper crucible and water cooled, non-consumable tungsten electrode and an argon-controlled atmosphere. These ingots were melted 5 times to ensure an homogeneous chemical composition. The cooling was done in furnace at rate of 5 °C/min. The Ti-10Nb alloy was machined into 9 mm diameter and 120 mm long cylinders. The cylindrical samples were heat-treated at 1000 °C for 24 h in argon atmosphere, applying a rate of 5 °C/min followed by slow cooling rates to relieve residual tensions originated on the fusion process.

The pure Ti, pure Nb, and Ti-10Nb alloy phases were determined by X-ray diffraction (Bruker—D8 Advance diffractometer with LYNXEYE-XE detector), operating at 40 kV and 20 mA, Cu K α radiation, in Bragg-Brentano geometry (2θ – 20–80°) in step scan of 2° min^{-1}. The microstructure, chemical composition and distribution of elements in Ti-10Nb alloy were analyzed by scanning electron microscopy (SEM, FEI Quanta 450 FEG) coupled to energy-dispersive X-ray spectroscopy (EDS).

The samples surfaces were ground with SiC papers and polished with colloidal silica. They were then degreased by sonicating in acetone, isopropyl alcohol and deionized water, for 15 min in each bath, and finally dried in an incubator at 40 °C for 24 h. Anodic oxidation was carried out in a two-electrode electrochemical cell, using a platinum wire as counter electrode and the Ti-10Nb samples as work electrode. The anodic film were obtained using an aqueous solution of 1.0 M H_3PO_4 + 0.8 wt% NH_4F as electrolyte. The anodization was conducted at constant voltage of 20 V for 40 min at room temperature. Some anodized samples were submitted to a subsequent thermal treatment. After the anodization, these samples were washed with deionized water, dried, and calcined for 3 h at 530 °C, 430 °C or 230 °C at a heating rate of 1 °C per minute, and cooled in the oven.

The morphology and the thickness of the anodic film were observed by SEM images. In particular, the thickness was observed in the SE (Secondary Electron) and BSE (Backscattering Electron) modes. Image J software was used to measure the film length on images of mechanically cracked samples. The chemical composition and distribution of elements in the anodized Ti-10Nb alloy were analyzed by EDS in line mode.

The X-ray diffraction equipment (Bruker – D8 Advance, LYNXEYE-XE detector) was used to identify the phases of oxide formed on Ti-10Nb alloy after the anodic process and after annealing at different temperatures. Due to the low film thickness the grazing X-ray incidence angle technique was employed at θ = 3°, divergence slit of 1.0 mm and 1.56% nickel filter was used to cut the K_β radiation, at 40 kV and 20 mA, Cu K α radiation.

The morphology, thickness and pattern of diffraction of nanostructured film were also investigated by transmission electron microscopy (TEM -JEOL JEM 1200EX-II), operated at 120 kV. For the TEM and SAED (Selected Area Electron Diffraction) analyses, the nanostructured film was removed from the plate of Ti-10Nb alloy using a paper stiletto, and then it was placed on the copper grid. After that, it was dripped one drop of the distilled water, on the copper grid with the nanostructured film, and then dried in an incubator at 40 °C for 24 h.

Surface wettability was evaluated on polished samples and on anodic film before and after annealing, using a contact-angle goniometer (EasyDrop, Krüss) in sessile drop mode with 1 μL PBS (phosphate-buffered saline) drops. The contact angles within 1 s were monitored and the average of three measurements was analyzed. The wettability results were compared also with results of a nanostructured film obtained using a 0.5 M Na2SO4 + 0.1%wt HF electrolyte that was characterized in a previous research [26], since both films, have similar morphologies and oxide compositions. The wettability behavior was investigated for as-prepared nanostructured film and after annealing at 230 °C for 3 h., for films obtained using distinct electrolytes.

3. Results and discussions

Fig. 1 shows the XRD pattern of the pure Ti, pure Nb and of the Ti-10Nb alloy. As expected, pure Ti showed only peaks correspondent to α phase, whereas pure Nb showed peaks of the β phase. The dots line correspond to β phase in the Ti-10Nb alloy. All the others peaks of the Ti-10Nb alloy are the contribution of the α phase. The presence majority of the α phase in Ti-10Nb alloy is due to the low amount of the β stabilizer element [39]. During the fabrication, the

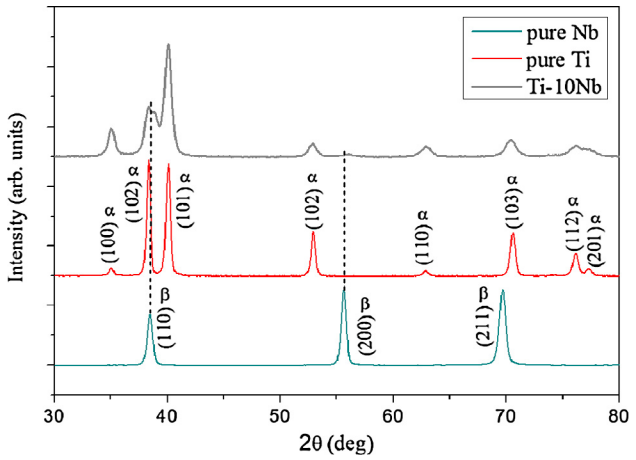

Fig. 1. X-ray diffraction pattern of the polished surfaces: pure Ti, pure Nb, and Ti-10Nb alloy.

alloy was heated above the beta transus temperature, but due to the slow cooling rate (α + β) phases are produced, resulting in a retained β structure [39]. The typical Ti-10Nb lamellar structure can be observed on the SEM image (Fig. 2a), where light regions are rich in β-phase and the dark regions are rich α-phase, in agreement to operating principles of SEM. This microstructure is characteristic of alloys compound by (α + β) phases [4,28,40], which can improve the mechanical properties of Ti and its alloys [1]. The Nb addition on Ti alloy can increse the strength and reduce the elastic modulus [1,5]. As reported in a previous research [26], the elastic modulus values obtained by instrumented indentation were (131 ± 4) GPa for grade 2 Ti and (110 ± 2) GPa for Ti-10Nb alloy. Therefore, the addition of Nb in the Ti-10Nb alloy can reduce the stress shielding effect that is responsible for bone resorption, loosening, and eventually replacement surgeries [1,5].

The manufactured alloy presented a homogeneous element distribution (Fig. 2b). Niobium is distributed over all the alloy microstructure, being more concentrated in β phase regions (circles on Fig. 2). The element weight percentage obtained by EDS analysis for Ti-10Nb alloy were (91 ± 4) and (9 ± 3) for Ti and Nb, respectively.

Fig. 3(a,b) show SEM images of the film morphology on the Ti-10Nb alloy. It is possible to observe the well-defined nanotubes presence just grown on α phase regions, as grown on pure Ti or monophasic alloys [8,41]. Whereas, on regions rich in β, α phase lamellar structure was observed.

This phenomenon was already described from previous research [26], and different morphologies were also observed in reports for nanotubes grown on biphasic (α + β) alloys [16,23–25]. Luz et al. [26] showed the first results about nanotubes grew on Ti-Nb alloy surface. They reported the influence of microstructure on the nanostructured film, tube like shape are formed on α phase and lamellar structure with transversal holes on β phase of the Ti-10Nb alloy; obtained using saline electrolyte by anodic process. On the other hand, Berger et al. [25] obtained nanotubes on refractory metals (Al, TiAl3, TiAl, Ti3Al and Ti), due to the composition of alloys two distinct morphologies were observed: (i) highly ordered parallelly aligned porous oxide structures and (ii) ordered arrays of oxide nanotubes.

The mechanisms for the formation and growth of the nanotube structure is describe as the competition between two processes; the oxidation of valve metals to form oxides and chemical dissolution of oxides at the oxide/electrolyte interface [10,12,42]. Because of the chemical differences between the phases of Ti alloys, the electrolyte may etch one of the phases preferentially, so different dissolution rates can occur [12,24,25,43–47]. As a result, a non-uniform morphology of the nanostructured film can be observed

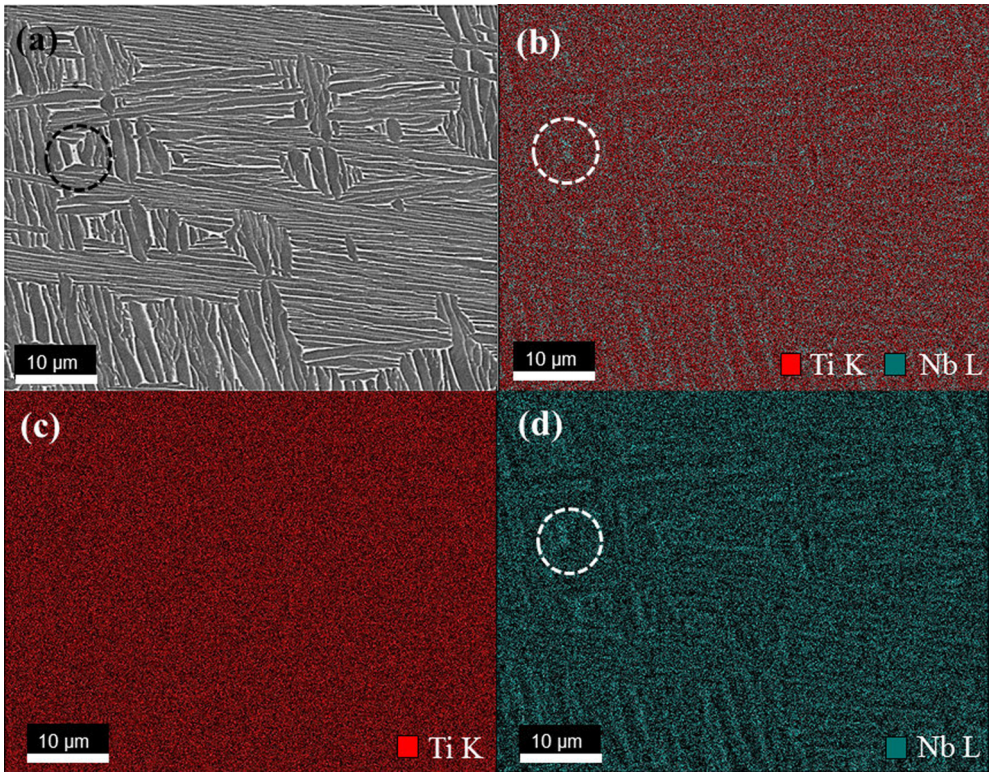

Fig. 2. Polished surface Ti-10Nb alloy: SEM image (a); EDS analysis on the surface showing: chemical map identifying Ti and Nb (b), distribution of each element in the chemical map Ti K (c) and Nb L (d).

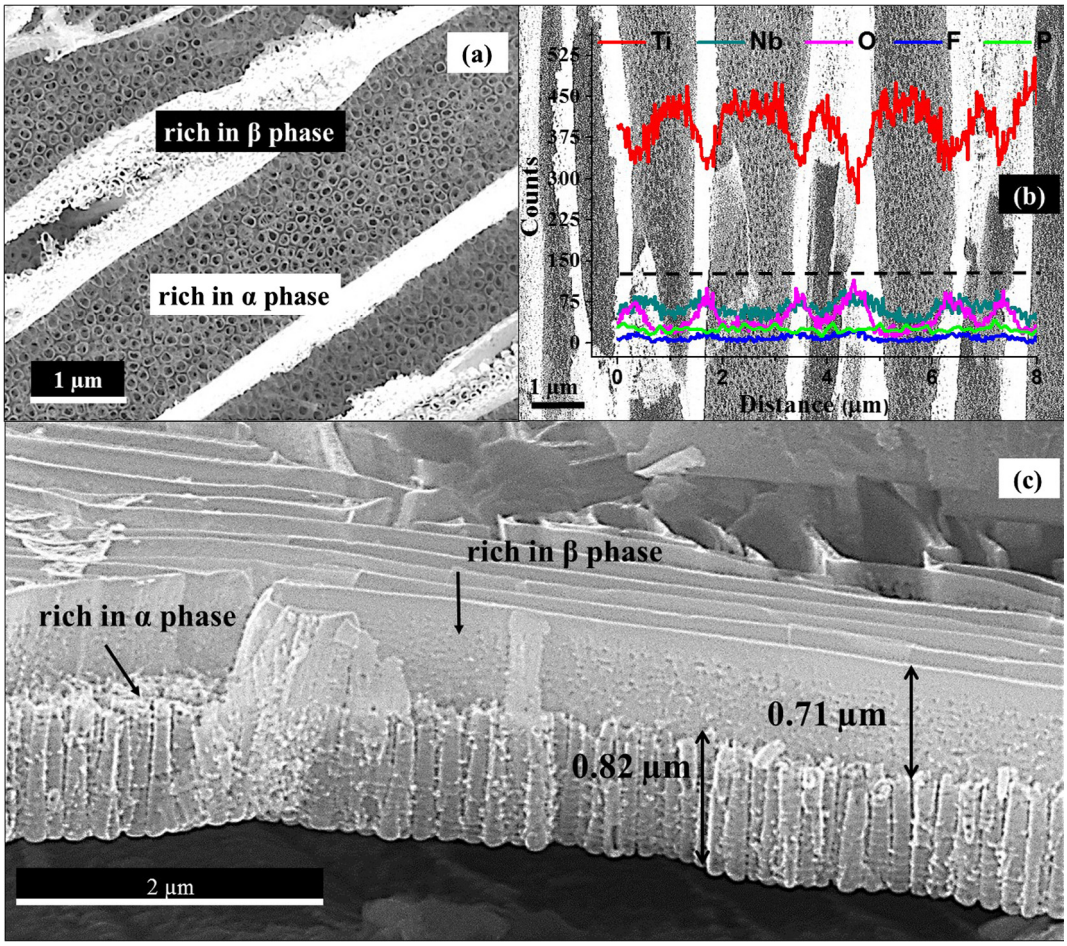

Fig. 3. Morphology of the Ti-10Nb alloy anodized at 20 V in 1 M H_3PO_4 (a) and (b); the insert in (b) is the EDS counts for elements in the nanostructured film in line mode measured at the black dot line region, and cross-sectional view of nanotube arrays (c).

on the biphasic alloys. Therefore, the Ti-10Nb alloy regions rich in α phase (Fig. 3) was etched preferentially in relation to regions rich in β phase, explaining the presence of uniformly distributed and self-organized nanotubes grown on the regions rich in α-phase.

The insert in Fig. 3b corresponds to the EDS analysis obtained in line mode to investigate the chemical composition of the nanostructured film grown on the Ti-10Nb alloy. The dot line region in the Fig. 3b indicated the analyzed region. The data reveals the contribution of substrate elements (Ti and Nb), F and P ions of electrolyte were incorporated in the film and the presence of O; due to the oxide formation by anodic process [48].

The light gray regions present higher Nb concentration than dark gray regions (Fig. 3b). Unlike, Ti concentration decreases in the light gray regions and increases in the dark gray regions. Therefore, the dark regions are rich in α-phase and the light regions are rich in β-phase, in agree with Fig. 2, since the Nb is a beta stabilizer element [39,49].

The counts for oxygen, fluorine of the regions rich in β phase was higher than in regions rich in α phase while the P counts are higher in the α regions. The lamellar structure is narrow (Fig. 3) and under it there is the nanotube arrays of α phase (Fig. 3c), so the results of EDS analysis may be influenced for both phases.

In agreement to Bauer et al. [25], PO_4^{3-} ions are adsorbed strongly on TiO_2 surfaces obtained with electrolyte containing phosphoric acid. They observed the presence of ≈4% of P on the surface of anodic TiO_2 surface grown on titanium (in absence of fluorides) in the H_3PO_4 solution by XPS analysis. In the same way, Ghicov et al. [32] observed phosphate ions incorporation into the nanotubes obtained with 1 M $(NH_4)H_2PO_4$ + 0.5 wt% NH_4F on pure Ti. The film contained ~2% of the phosphorous species (~8% phosphates) by XPS analysis. Despite the phosphorus incorporation into the film grew on the Ti-10Nb alloy was done by EDS analysis, it is possible that this data is in agreement with XPS analysis reported by Bauer et al. [25] and Chicov et al. [32], since a low counts for phosphorous was obtained (Fig. 3b).

Furthermore, it is also well knew that incorporation of phosphates in oxide titanium suggest the presence of negatively charged species [29,32,50]. For example, HPO_4^- and PO_4^- can act as preferential nucleation sites of calcium phosphates due to attractive interaction with Ca^{2+} ions presents in biological fluid [50]. Recently, Sánchez-Escobedo et al. [51] showed the *in vitro* bioactivity of phosphorous-containing calcium monoaluminate cements increased by adding phosphorous.

To investigate the difference of the anodic film grown on α or on β regions, the cross-section of the sample was analyzed revealing different length in each region (Fig. 3c). The cross-section image shows that on the α-phase region nanotube arrays grown with ~0.82 μm of length and on the β-phase region a lamellar structure, likewise as observed in Fig. 3c.

In addition, the nanotubes on α-phase showed the growth of ribs along the tubes walls, which can be formed in aqueous electrolyte with regular current oscillations recorded in the current-time transient, associated with pH bursts at the base of the tubes as the anodization progressed [10]. Moreover, the presence of

NH_4F into electrolyte may be formed the ribs along the tubes walls [30,52].

The oxides formed on each one of the phases have different concentrations of Nb [24,26], in agree with Figs. 2 and 3b. The attack of the fluorine ions in the oxides on the alpha phase is different from the attack in the oxides on the beta phase [24,26]. The oxide layer grew on the beta phase is less attacked, with thickness ~0.71 μm higher than the nanotubes of the alpha phase oxides, probably due to oxide composition.

Berger et al. [25] attributed the transition from nanopores to nanotubes, for films grew on refractory metals (Al, TiAl3, TiAl, Ti3Al and Ti), to the oxide growth factor f_{growth} proposed by Yasuda et al. [45]. The f_{growth} denote the proportionality between thickness t and anodization voltage U for the growth of compact valve metal oxide layers [$t = f_{growth}U$]). The model implicate that the tube diameter (d_{tube}) of self-organized nanotubes arrays on several valve metals essentially depends on the oxide growth factor f_{growth}, which is express by $d_{tube} = 2f_{growth}U$ [45].

The f_{growth} may be related to stress generated during oxide formation and depends on the volume expansion during oxide growth [29]. Therefore, the different morphologies and thickness observed in Fig. 3 may be attributed to the f_{growth}, since the oxide composition is different on α and β phase and the growth of compact oxide is also different on phases of the Ti-10Nb alloy [26].

Fig. 4 shows the TEM, SEM- BSE and SAED results in order to investigate the oxide composition of the nanostructured film in relation of the different morphologies (Fig. 3). A significant relationship was observed between the film thickness and the features morphology obtained by TEM (Fig. 4a) and the SEM images (Fig. 4b), since the order of magnitude is close to 2 μm for the two results. Both TEM and SEM images (Fig. 4a,b) show a nonporous edge (1) and region with tubes (3).

The TEM image (Fig. 4a) clarified the characteristics of the region with holes (2) that have random diameters, which increase of size from the edge towards to the region with tubes (3). So, the holes in the wall are affected by the neighboring tubes on the α phase. This behavior may be similar to the pore formation when the pores that precedes the formation of nanotubes affects the growth one of the others; and consequently the growth of nanotubes [45].

TEM images with different features of the nanostructured film were selected: tubes (c), lamellar structure showed the edge and holes (d) and the contribution of the all film (e), i.e., tubes plus lamellar structure. The patterns of the SAED (Fig. 4f–h) correspond to regions (Fig. 4c–e), respectively. All regions of the nanostructured film grown on Ti-10Nb showed diffuse rings and there are not define points to index to crystalline oxide patterns. Thus, it is an evidence that the nanostructured film is amorphous, independent of the region on it grown (α or β phases). As well known, the nanotubes grown by anodic process are amorphous, and it can turn crystalline by annealing [7,37,41].

Fig. 5 shows results after annealing of nanostructured film by SEM, EDS, TEM and SAED analyses.

In order to obtain higher crystallinity, the nanostructured film were annealed at 530 °C for 3 h. This condition of annealing was choice since it is frequently used to convert amorphous nanotubes to crystalline nanotubes rich in anatase phase without collapsing the nanotubes [53]. Fig. 5a shows the morphology of nanostructured film after this process. Unfortunately, the lamellar structure grown on β phase was destroyed after the annealing at 530 °C for 3

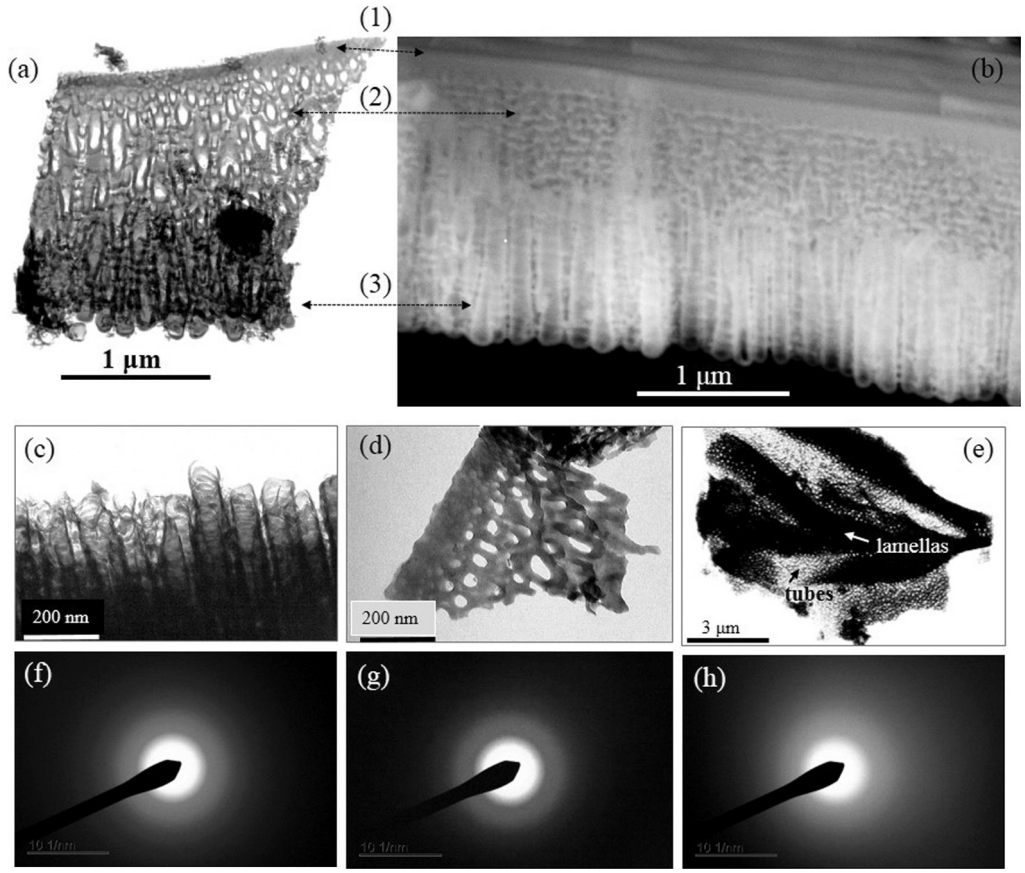

Fig. 4. Morphology/film thickness grown on the Ti-10Nb alloy obtained by TEM (a) and SEM - BSE. Different selected area of the nanostructured film: tubes (c), lamellar structure (d) and tubes plus lamellar structure (e). Pattern of the SAED (f–h), which correspond the fig. c–e, respectively.

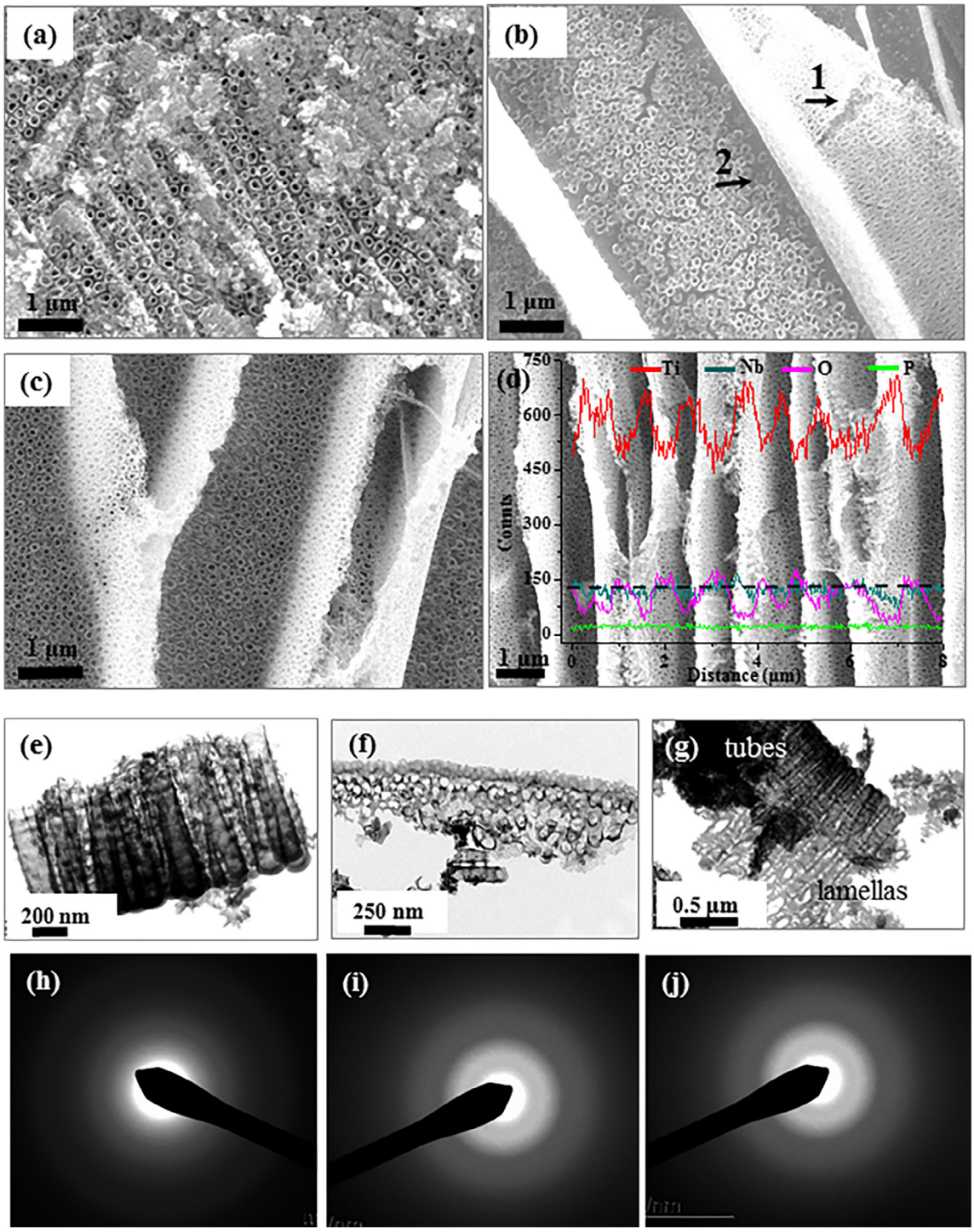

Fig. 5. Morphology of nanostructured film grown on the Ti-10Nb alloy after annealing by SEM: (a) 530 °C for 3 h, (b) 430 °C for 3 h, (c) 230 °C for 3 h. The insert in (d) is the EDS counts in line mode for elements in nanostructured film after annealing at 230 °C for 3 h, the black dot line is the region analyzed. Morphology of different selected area of nanostructured film after annealing at 230 °C for 3 h by TEM: tubes (e), lamellar structure (f) and tubes plus lamellar structure (g). Patterns of the SAED (h–j), which correspond the fig. e–g, respectively.

h. Reducing the annealing temperature to 430 °C for 3 h, it was observed cracks on lamellar structure (Fig. 5b, 1-black arrow) and a region with collapsed nanotubes grown on α phase close to lamellar structure (Fig. 5b, 2-black arrow).

Reducing the annealing temperature to 230 °C for 3 h the nanostructured film (Fig. 5c) was uniform over the substrate; it were not observed cracks or collapsed regions. Therefore, the nanostructured film was not damaged in this condition, so complementary analyses were done.

The insert in Fig. 5d corresponds to the EDS analysis obtained in line mode to investigate the chemical composition after annealing at 230 °C for 3 h. The data reveals that the fluorine ions were removed of film and the others elements (Ti, Nb, O and P) showed the same features that Fig. 3b.

In order to investigated the crystallinity of nanostructured film after the annealing at 230 °C for 3 h TEM and SAED analyses were done. Fig. 5e–g show these morphologies: tube, lamella or tube plus lamellar maintained the same features before the annealing

(comparing Figs. 4 and 5), and the SAED patterns (Fig. 5h–j) are still amorphous.

Nanotube grown on pure Ti showed that anatase formation begins at around 280 °C [8], and increasing annealing temperature the anatase formation can be enhanced. However, the alloying elements can change the phase transformation temperature [8]. Nanotubes grown on alloys containing Nb, Al, Ni, Ga, Ta, and W and submitted to annealing shows retards to formation of anatase and rutile crystallites and delays the anatase-to-rutile phase transformation [8]. Verissimo et al. [54] observed by X-ray diffraction patterns two peaks of anatase to nanotubes grown on pure Ti annealing at 225 °C with low intensity, whereas the nanotubes grown on Ti-35Nb alloy shows a low intensity to one peak of anatase after annealing at 295 °C.

The temperature of 230 °C has selected in according the results of Verissimo et al. [54], in order to promote a minimum changes at structure crystalline, maintained morphology of as-prepared nanostructure film and remove the fluorine ions, since that the unannealed film had a crystalline contribution of the oxide formed in the oxide-metal interface, as showed by XRD patterns (Fig. 6).

Fig. 6 shows the peaks on the XRD patterns of the Ti-10Nb substrate in comparing to the anodized Ti-10Nb alloy, and after annealing at different temperatures. In relation to pure Ti-10Nb alloy, as-prepared nanostructured surface showed significant change at peaks of the anatase at 48°, overlapping anatase peaks with substrate at 38.5°, 55.7° and 62.7°, Nb_2O_5 at 29° and 43°. The presence of crystalline peaks of the XRD patterns (Fig. 6) can be attributed to the oxide formation in the oxide-metal interface [26,48,55,56], since the SAED results showed the lamellas and tubes are amorphous.

Furthermore, the EDS analysis (Figs. 3 and 5) suggest that the nanostructured film on Ti–10Nb alloy can be formed of TiO_2 and Nb_2O_5 oxides. Moreover, films grew by anodization may lead to the formation of niobium oxides; being that depends of preparation conditions [57].

The oxidized surface annealed at 230 °C shows that anatase peaks at ~38° were more defined than as-prepared film, and a broad region from 7° to 18° of Nb_2O_5 peaks, which are also remained at other annealing conditions (430 °C and 530 °C). At 430 °C additional anatase peak was observed at ~25°, but at ~55.7° the anatase peak was suppressed. The same oxide contribution was observed on anodic film annealed at 530 °C, being that all peaks were more defined than 430 °C.

Nanotubes grown on Ti-35Nb alloy showed that the anatase phase starts the crystallization at 325–350 °C [54], which can explain the formation of the typical anatase peak ~25° (Fig. 6). Whereas, the higher crystallization of Nb_2O_5 powder was observed at 500 °C [58], peaks of Nb_2O_5 were obtained at 480–930 °C for nanotubes grown on Ti-35Nb alloy [54], and nanotube arrays grown on Ti-45Nb alloy showed highly crystalline Nb_2O_5 after annealing at 550 °C [59]. These data of literature are indicatives of the lower crystallinity of Nb2O5 peaks observed after annealing (230–530 °C) in Fig. 6, as well as, it changed at crystalline structure of the as-prepared nanostructured film on Ti-10Nb alloy. However, due to extensive polymorphism of niobium oxides is not possible comparing data. Furthermore, the formation of Nb oxides depends of substrate, on the method of preparation and annealing conditions [57].

Therefore, increasing the annealing temperature the crystallinity of anatase phase of nanostructured film was enhanced [8]. However, the different morphologies (tubes and lamellas) of film grown on Ti10Nb alloy were damaged at higher temperatures (Fig. 5).

The deterioration of nanotube arrays due to annealing can depend of experimental parameters, as anodization condition, temperature, hold time for thermal degradation, phase transformation and crystallization of nanotubes [60]. Shivaram et al. 2014 [60] also observed that the length tubes can lead to thermal degradation at lower temperatures of nanotubes. In this work, the deterioration of nanotubes can also be associated to differences at morphologies and their oxide composition.

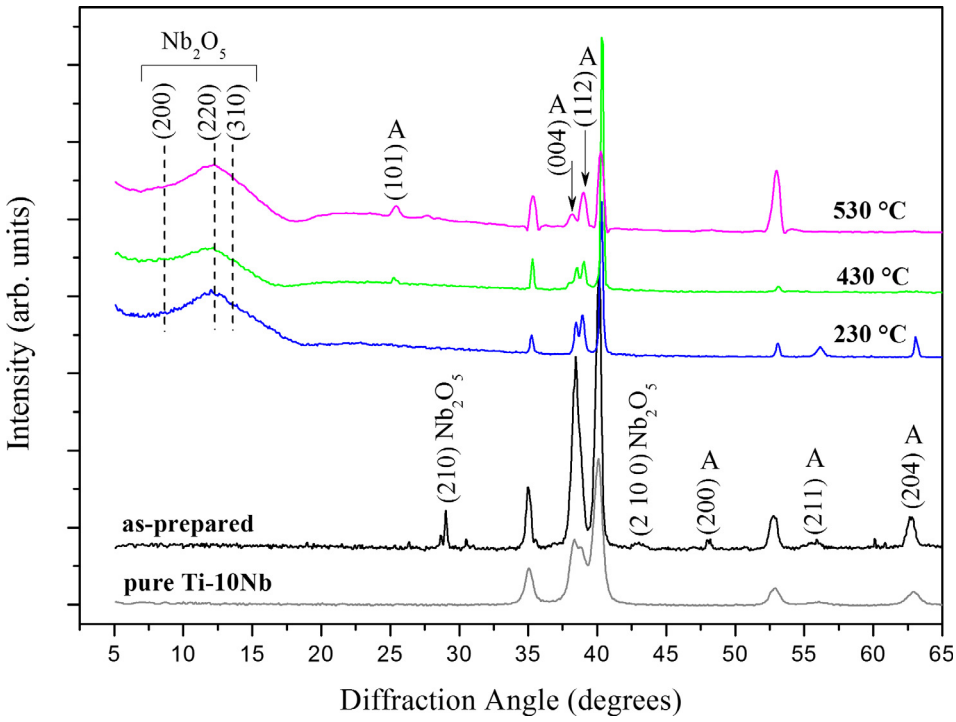

Fig. 6. X-ray diffraction spectra: pure Ti-10Nb, as-prepared anodized Ti-10Nb alloy and after annealing at different temperatures (230 °C, 430 °C and 530 °C). "A" correspond to anatase peaks.

At last, Fig. 6 showed that the nanostructured film (as-prepared and after annealing) was formed by mixtures of oxides of elements that compound the alloy [8,48]. Titanium and niobium oxides show bioactivity *in vitro* and *in vivo* tests [61,62], whereas it was demonstrated that amorphous nanotubes are adequate surfaces for cell adhesion [63,64]. Being that the anatase phase may to enhance the growth process of hydroxyapatite [56]. Besides that, coatings with TiO_2 and Nb_2O_5 oxides can improve the corrosion resistance and the wear [42,58].

Therefore, a nanostructured film as obtained in this work probably have suitable characteristics for applications in biomaterials area. In fact, the evaluation of biological response of nanostructured film with lamellas and tubes should be investigated in future research, since the surface morphology is decisive to cell interaction between bone and implant [56].

Fig. 7a shows that the contact angle of PBS on polished Ti-10Nb alloy is approximately 57° (Fig. 7a), on this alloy were grown nanostructured film using distinct electrolytes. In the previous research [26] the film was grown with 0.5 M Na_2SO_4 + 0.1% wt HF electrolyte, which morphology had lamellas and tubes. In this work, a similar nanostructured film obtained with 1 M H_3PO_4 + 0.8 %wt NH_4F electrolyte also had lamellas and tubes (Figs. 3–4). The similar morphologies observed in Figs. 3–4 and in previous research [26] were expressed in a schematic drawing showed in Fig. 7b. Although these nanostrutured films had a similar morphology and oxide composition (titania and niobia oxides), the wettability of these surface were very different (Fig. 7c,d).

Fig. 7c shows that as-prepared surface obtained with 0.5 M Na_2SO_4 + 0.1%wt HF electrolyte had almost hydrophobic behavior with contact angle (78° ± 2°). After the annealing at 230 °C for 3 h, the contact angle increased and showed a hydrophobic surface (Fig. 7c) with (104° ± 3) contact angle. Whereas, when 1 M H_3PO_4 + 0.8 %wt NH_4F electrolyte was employed to obtain the nanostructured film, as-prepared and after annealing surfaces revealed a hydrophilic behavior with (19° ± 2°) and (37° ± 2°) contact angle, respectively (Fig. 7d).

Fig. c-I shows a scheme for a low surface energy that correspond the behavior of the nanostructured film obtained with Na_2SO_4 + HF electrolyte, wich the liquid does not permate into the film due to air pockets there are beetwen the liquid and solid surface; as describe by the Cassie and Baxter model [65,66].

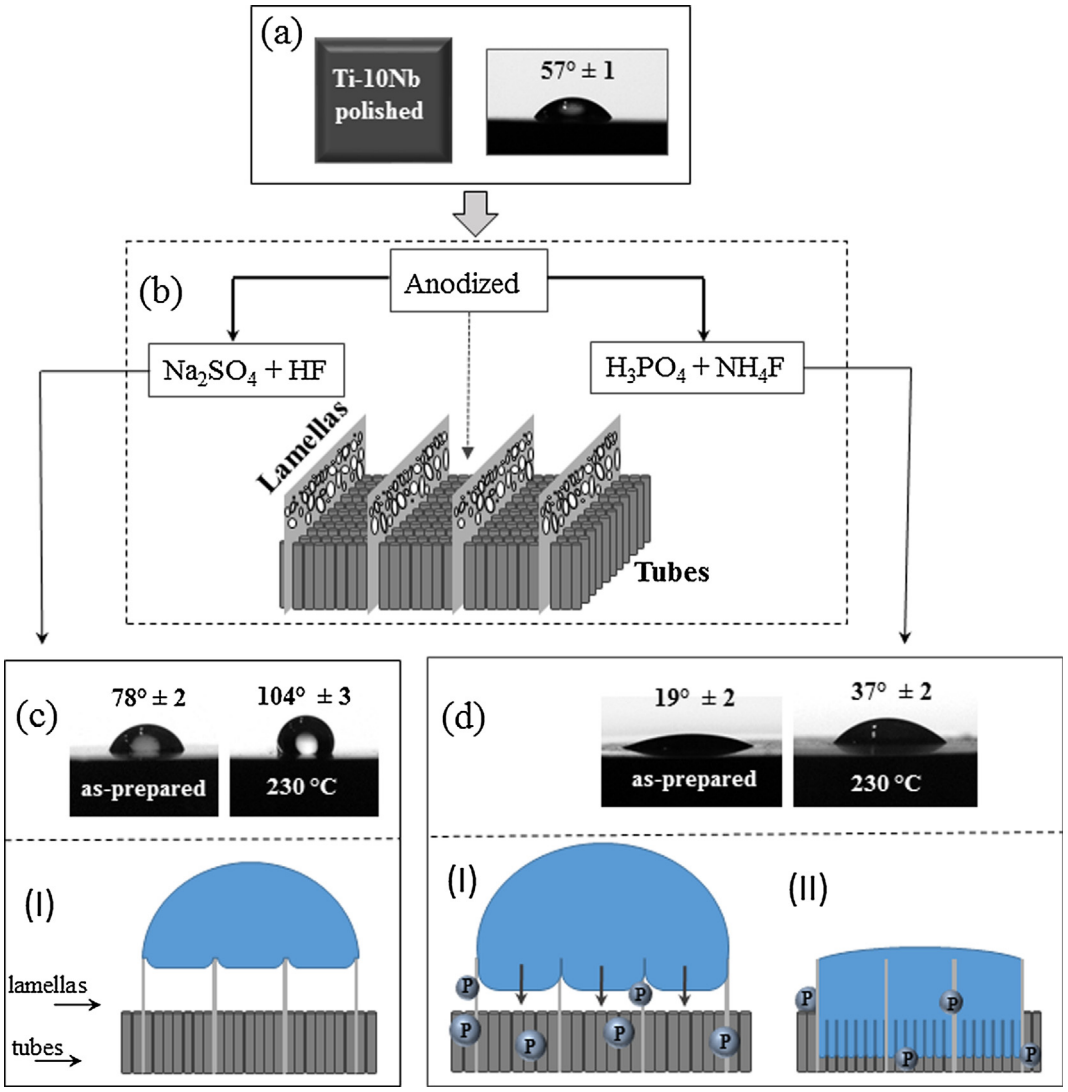

Fig. 7. Contact angle measurements of Ti-10Nb polished (a), schematics of morphology obtained with different electrolytes (b), contact angle measurements of as-prepared surface and before annealing at 230 °C of nanostructured film on Ti-10Nb alloy grown using Na_2SO_4 + HF electrolyte (c) and H_3PO_4 + NH_4F eletrolyte (d). Schematics of wetting behavior: hydrophobic surface (c-I), hydrophilic surface when start of wetting of fluid into film (d-I) and complete wetting (d-II). The circles with "P" on (d-I) and (d-II) are phosphorus incorporation.

Whereas, Fig. d-I shows a schematic for a hydrophilic surface when start of wetting of fluid into film. Perhaps, the phosphorous incorporation increase the surface energy, and then the nanostructured film obtained with $H_3PO_4 + NH_4F$ was entirely wetted by liquid droplet (d-II), which is in accordance with Wenzel model [66].

A hydrophilic behavior of nanotubes surface can be expected, due to an increase of roughness, surface area in relation flat surfaces and reaction with hydroxide compounds on nanotubes surfaces [34,37]. However, the surface chemistry controls the surfaces properties, those could be changed depend on the processing method and heat treatment. Thus, a hydrophobic behavior can be observed for nanostrucured films [37,56,60].

The increase on the contact angle after annealing is reported in literature due to the adsorption of organic contaminants on nanostructured surface in air ambience and the replacement of the chemisorbed hydroxyl groups with the oxygens [65].

Both the surface morphology and the crystalline structure can influence the surface wettability, as well as, surface energy [56]. In the way, Yavari et al.[24] attributted the low contact angle to the porous morphology and films roughness, and the presence of anatase, rutile and oxides of elements that compound the α/β-Ti6Al7Nb and β-Ti45Nb alloys. Furthermore, nanotube surface compound by crystalline anatase showed best wettability than amorphous oxide and rutile phase [56].

However, these characteristics, surface morphology and crystalline structure, were not decisive in wettability behavior of nanostructured films analyzed in this work. The most important difference between the nanostructured films contained lamellas and tubes was the phosphorous incorporation that, probably, change the surface chemistry and the free energy to turn the surface hydrophilic. This fact can be emphasized observing data of others researches and our research group that have been observing the presence of phosphorous on the anodic surface seems improve the hydrophilicity. For porous films obtained by plasma electrolytic oxidation [24,35,36] it was observed that the incorporation of phosphorus plays decisive role to surface hydrophilicity.

Due to the complexity of surface effects of thin films [56], further studies are necessary to fully comprehend this behavior, such as an extensive review of literature data, many wettability tests of surface obtained using different electrolytes, as well as the complete characterization of all surfaces (surface chemistry and free energy).

In view of wettability results, films obtained using electrolytes contained phosphorous ions can show a low contact angle, which suggests a high surface energy of films. The higher hydrophilicity and surface energy of anodized surface improved the apatite-forming ability in SBF (simulated body fluid). In addition, the nanotube structure is more reactive due to a more open surface area leading to enhanced apatite deposition [67]. The increased hydrophilicity improves the surface-blood interaction, increase the protein adsorption and consequently, modulate the cell growth and differentiation [42,68]. The higher wettability also results on an increased anti-inflammatory response, resulting in a reduced healing time [69].

Therefore, the nanostructured film obtained with $H_3PO_4 + NH_4F$ eletrolyte can had optimize of the physic-chemical surface properties of the Ti-10Nb alloy. The combination of the morphology characteristics, the presence of the anatase phase and the phosphorous incorporation may be improved surface wettability. The analyses of the phosphorus incorporation (Fig. 3b and 5d) and of the surface wettability (Fig. 7) showed an insight to need more investigations to understand the relationship between the low contact angle and the incorporation of phosphorous in anodic films.

4. Conclusions

The present study showed that the oxides formed on α and on β phases of Ti-10Nb alloy have different nanostructured morphology, chemical composition and thickness that are result from an uneven grow. On α- type regions self-organized nanotubes grown, whereas on β-type regions a lamellar structure with transversal holes was formed with a higher thickness than for nanotubes on α phase oxides. Crystalline oxide formation was observed near to oxide-metal interface, whereas the tubes and lamellas grown over the compact crystalline oxide phases are amorphous, as-prepared and annealing at 230 °C for 3 h. The nanostructured film was damaged when submitted to annealing at 430 °C or 530 °C, whereas at 230 °C the morphology was similar as unannealed surface and a few changes were observed in structure by XRD patterns. An increase in the surface wettability of the film was observed in comparison with the polished alloy, attributed not only to the morphology, but also to the anatase phase and the phosphorus ions incorporated into the anodic layer, since a similar nanostructured film without phosphorous incorporation was hydrophobic.

Acknowledgements

The authors would like to thank the Centro de Microscopia da UFPR, the LORXI - Laboratório de Óptica de Raios X e Instrumentação do Departamento de Física da UFPR, LaBES – Laboratório de Biomateriais e Engenharia de Superfícies PUC-PR and Laboratório de Anelasticidade e Biomateriais (LAB-UNESP/Bauru) for the facilities, the Fundação Araucária (n.° 685/2014, project 42466), CNPQ and CAPES for financial support.

References

[1] J.M. Cordeiro, V.A.R. Barão, Is there scientific evidence favoring the substitution of commercially pure titanium with titanium alloys for the manufacture of dental implants?, Mater Sci. Eng. C 71 (2017) 1201–1215, https://doi.org/10.1016/j.msec.2016.10.025.
[2] Y. Okazaki, E. Gotoh, Comparison of metal release from various metallic biomaterials in vitro, Biomaterials 26 (2005) 11–21, https://doi.org/10.1016/j.biomaterials.2004.02.005.
[3] A.M. Cortizo, L. Bruzzone, S. Molinuevo, S.B. Etcheverry, A possible role of oxidative stress in the vanadium-induced cytotoxicity in the MC3T3E1 osteoblast and UMR106 osteosarcoma cell lines, Toxicology 147 (2000) 89–99, https://doi.org/10.1016/S0300-483X(00)00181-5.
[4] M. Nakai, M. Niinomi, K. Cho, K. Narita, Enhancing functionalities of metallic materials by controlling phase stability for use in orthopedic implants, in: Interface Oral Heal. Sci. 2014, Springer Japan, Tokyo, 2015, pp. 79–91. http://doi.org/10.1007/978-4-431-55192-8_7.
[5] M. Niinomi, Y. Liu, M. Nakai, H. Liu, H. Li, Biomedical titanium alloys with Young's moduli close to that of cortical bone, Regen. Biomater. 3 (2016) 173–185, https://doi.org/10.1093/rb/rbw016.
[6] R. Zhang, Y. Wan, X. Ai, B. Men, T. Wang, Z. Liu, D. Zhang, Fabrication of micro/nano-textured titanium alloy implant surface and its influence on hydroxyapatite coatings, J. Wuhan Univ. Technol. Sci. Ed. 31 (2016) 440–445, https://doi.org/10.1007/s11595-016-1389-5.
[7] M. Kulkarni, A. Mazare, E. Gongadze, S. Perutkova, V. Kralj-Iglic, I. Milosev, P. Schmuki, A. Iglic, M. Mozetic, Titanium nanostructures for biomedical applications, Nanotechnology. 26 (2015) 62002 (1–18). http://doi.org/10.1088/0957-4484/26/6/062002.
[8] P. Roy, S. Berger, P. Schmuki, TiO2 nanotubes: synthesis and applications, Angew. Chem. Int. Ed. Engl. 50 (2011) 2904–2939, https://doi.org/10.1002/anie.201001374.
[9] Y. Yang, Y. Lai, Q. Zhang, K. Wu, L. Zhang, C. Lin, P. Tang, A novel electrochemical strategy for improving blood compatibility of titanium-based biomaterials, Colloids Surf. B Biointerfaces 79 (2010) 309–313, https://doi.org/10.1016/j.colsurfb.2010.04.013.
[10] D. Regonini, C.R. Bowen, A. Jaroenworaluck, R. Stevens, A review of growth mechanism, structure and crystallinity of anodized TiO_2 nanotubes, Mater. Sci. Eng. R Reports. 74 (2013) 377–406, https://doi.org/10.1016/j.mser.2013.10.001.
[11] G.A. Crawford, N. Chawla, Porous hierarchical TiO_2 nanostructures: processing and microstructure relationships, Acta Mater. 57 (2009) 854–867, https://doi.org/10.1016/j.actamat.2008.10.032.
[12] G.A. Crawford, N. Chawla, Tailoring TiO_2 nanotube growth during anodic oxidation by crystallographic orientation of Ti, Scr. Mater. 60 (2009) 874–877, https://doi.org/10.1016/j.scriptamat.2009.01.043.

[13] S. Leonardi, A.L. Bassi, V. Russo, F. Di Fonzo, O. Paschos, T.M. Murray, H. Efstathiadis, J. Kunze, TiO_2 Nanotubes: interdependence of substrate grain, J. Phys. Chem. 116 (2012) 384–392, https://doi.org/10.1021/jp209418n.

[14] S. Leonardi, V. Russo, A. Li Bassi, F. Di Fonzo, T.M. Murray, H. Efstathiadis, A. Agnoli, J. Kunze-Liebhäuser, TiO_2 nanotubes: interdependence of substrate grain orientation and growth rate, ACS Appl. Mater. Interfaces 7 (2014) 1662–1668, https://doi.org/10.1021/am507181p.

[15] Z. Su, L. Zhang, F. Jiang, W. Zhou, Z. Deng, Y. Cao, M. Hong, Formation of anodic TiO_2 nanotube arrays with bimodal pore size distribution, Electrochem. Commun. 31 (2013) 67–70, https://doi.org/10.1016/j.elecom.2013.03.007.

[16] J.M. Macak, M. Jarosova, A. Jäger, H. Sopha, M. Klementová, Influence of the Ti microstructure on anodic self-organized TiO_2 nanotube layers produced in ethylene glycol electrolytes, Appl. Surf. Sci. 371 (2016) 607–612, https://doi.org/10.1016/j.apsusc.2016.03.012.

[17] H. Sopha, A. Jäger, P. Knotek, K. Tesa, M. Jarosova, J.M. Macak, Electrochimica acta self-organized anodic TiO2 nanotube layers : influence of the Ti substrate on Nanotube Growth and Dimensions, 190 (2016) 744–752. http://doi.org/10.1016/j.electacta.2015.12.121.

[18] U. König, B. Davepon, Microstructure of polycrystalline Ti and its microelectrochemical properties by means of electron-backscattering diffraction (EBSD), Electrochim. Acta 47 (2001) 149–160, https://doi.org/10.1016/S0013-4686(01)00572-2.

[19] B. Davepon, J.W. Schultze, U. König, C. Rosenkranz, Crystallographic orientation of single grains of polycrystalline titanium and their influence on electrochemical processes, Surf. Coat. Technol. 169–170 (2003) 85–90, https://doi.org/10.1016/S0257-8972(03)00163-4.

[20] L.E. Fratila-Apachitei, H. Terryn, P. Skeldon, G.E. Thompson, J. Duszczyk, L. Katgerman, Influence of substrate microstructure on the growth of anodic oxide layers, Electrochim. Acta 49 (2004) 1127–1140, https://doi.org/10.1016/j.electacta.2003.10.024.

[21] E. Matykina, R. Arrabal, P. Skeldon, G.E. Thompson, H. Habazaki, Influence of grain orientation on oxygen generation in anodic titania, Thin Solid Films 516 (2008) 2296–2305, https://doi.org/10.1016/j.tsf.2007.08.104.

[22] M.V. Diamanti, M.P. Pedeferri, C.A. Schuh, Thickness of anodic titanium oxides as a function of crystallographic orientation of the substrate, Metall. Mater. Trans. A Phys. Metall. Mater. Sci. 39 (2008) 2143–2147, https://doi.org/10.1007/s11661-008-9558-6.

[23] M.L. Vera, M.C. Avalos, M.R. Rosenberger, R.E. Bolmaro, C.E. Schvezov, A.E. Ares, Evaluation of the influence of texture and microstructure of titanium substrates on TiO_2 anodic coatings at 60 V, Mater. Charact. 131 (2017) 348–358, https://doi.org/10.1016/j.matchar.2017.07.005.

[24] S.A. Yavari, B.S. Necula, L.E. Fratila-Apachitei, J. Duszczyk, I. Apachitei, Biofunctional surfaces by plasma electrolytic oxidation on titanium biomedical alloys Surface Engineering, Surf. Eng. 32(6) (2016) 417. http://doi.org/10.1179/1743294415Y.0000000101.

[25] S. Berger, H. Tsuchiya, P. Schmuki, Transition from nanopores to nanotubes: self-ordered anodic oxide structures on titanium – aluminides, Chem. Mater. 20 (2008) 3245–3247, https://doi.org/10.1016/j.cossms.2007.08.004. (22).

[26] A.R. Luz, C.M. Lepienski, S.L. Henke, C.R. Grandini, N.K. Kuromoto, Effect of microstructure on the nanotube growth by anodic oxidation on Ti-10Nb alloy, Mater. Res. Express. 76408 (2017) 1–11, https://doi.org/10.1088/2053-1591/aa7d25.

[27] I.V.S. Yashwanth, I. Gurrappa, The effect of titanium alloy composition in synthesis of Titania nanotubes, Mater. Lett. 142 (2015) 328–331, https://doi.org/10.1016/j.matlet.2014.12.010.

[28] C.P. Ferreira, M.C. Gonçalves, R. Caram, R. Bertazzoli, C.A. Rodrigues, Applied surface science effects of substrate microstructure on the formation of oriented oxide nanotube arrays on Ti and Ti alloys, 285P (2013) 226–234. http://doi.org/10.1016/j.apsusc.2013.08.041.

[29] S. Bauer, S. Kleber, P. Schmuki, TiO_2 nanotubes: tailoring the geometry in H3PO4/HF electrolytes, Electrochem. Commun. 8 (2006) 1321–1325, https://doi.org/10.1016/j.elecom.2006.05.030.

[30] Y. Zhang, D. Yu, M. Gao, D. Li, Y. Song, R. Jin, W. Ma, X. Zhu, Growth of anodic TiO_2 nanotubes in mixed electrolytes and novel method to extend nanotube diameter, Electrochim. Acta 160 (2015) 33–42, https://doi.org/10.1016/j.electacta.2015.02.058.

[31] Y. Zhang, H. Fan, X. Ding, Q. Yan, L. Wang, W. Ma, Simulation of anodizing current-time curves and morphology evolution of TiO_2 nanotubes anodized in electrolytes with different NH4F concentrations, Electrochim. Acta 176 (2015) 1083–1091, https://doi.org/10.1016/j.electacta.2015.07.110.

[32] A. Ghicov, H. Tsuchiya, J.M. MacAk, P. Schmuki, Titanium oxide nanotubes prepared in phosphate electrolytes, Electrochem. Commun. 7 (2005) 505–509, https://doi.org/10.1016/j.elecom.2005.03.007.

[33] M. Sarraf, E. Zalnezhad, A.R. Bushroa, A.M.S. Hamouda, A.R. Rafieerad, B. Nasiri-Tabrizi, Effect of microstructural evolution on wettability and tribological behavior of TiO_2 nanotubular arrays coated on Ti-6Al-4V, Ceram. Int. 41 (2015) 7952–7962, https://doi.org/10.1016/j.ceramint.2015.02.136.

[34] E.S. Kim, Y.H. Jeong, H.C. Choe, W.A. Brantley, Formation of titanium dioxide nanotubes on Ti-30Nb-xTa alloys by anodizing, Thin Solid Films 549 (2013) 141–146, https://doi.org/10.1016/j.tsf.2013.08.058.

[35] B.L. Pereira, C.M. Lepienski, I. Mazzaro, N.K. Kuromoto, Apatite grown in niobium by two-step plasma electrolytic oxidation, Mater. Sci. Eng. C (2016), https://doi.org/10.1016/j.msec.2016.10.073.

[36] B. Leandro Pereira, A.R. da Luz, C. Maurício Lepienski, I. Mazzaro, N. Kazue Kuromoto, Niobium treated by plasma electrolytic oxidation with calcium and phosphorus electrolytes, J. Mech. Behav. Biomed. Mater. 77 (2017) 347–352, https://doi.org/10.1016/j.jmbbm.2017.08.010.

[37] G. Liu, K. Du, K. Wang, Surface wettability of TiO_2 nanotube arrays prepared by electrochemical anodization, Appl. Surf. Sci. 388 (2016) 313–320, https://doi.org/10.1016/j.apsusc.2016.01.010.

[38] A. Roguska, M. Pisarek, A. Belcarz, L. Marcon, M. Holdynski, M. Andrzejczuk, M. Janik-Czachor, Improvement of the bio-functional properties of TiO_2 nanotubes, Appl. Surf. Sci. 388 (2016) 775–785, https://doi.org/10.1016/j.apsusc.2016.03.128.

[39] ASM International, Titanium—Physical Metallurgy, Processing, and Applications, First, 2015, Ohio, 2015.

[40] W.G. Kim, H.C. Choe, Y.M. Ko, W.A. Brantley, Nanotube morphology changes for Ti-Zr alloys as Zr content increases, Thin Solid Films 517 (2009) 5033–5037, https://doi.org/10.1016/j.tsf.2009.03.165.

[41] S. Minagar, C.C. Berndt, J. Wang, E. Ivanova, C. Wen, A review of the application of anodization for the fabrication of nanotubes on metal implant surfaces, Acta Biomater. 8 (2012) 2875–2888, https://doi.org/10.1016/j.actbio.2012.04.005.

[42] V.S. Simi, N. Rajendran, Influence of tunable diameter on the electrochemical behavior and antibacterial activity of titania nanotube arrays for biomedical applications, Mater. Charact. 129 (2017) 67–79, https://doi.org/10.1016/j.matchar.2017.04.019.

[43] A. Michaelis, J.W. Schultze, Effect of anisotropy on microellipsometry in the Ti TiO_2 system, Thin Solid Films 233 (1993) 86–90, https://doi.org/10.1016/0040-6090(93)90067-Y.

[44] H. Tsuchiya, J.M. MacAk, A. Ghicov, L. Taveira, P. Schmuki, Self-organized porous TiO_2 and ZrO_2 produced by anodization, Corros. Sci. 47 (2005) 3324–3335, https://doi.org/10.1016/j.corsci.2005.05.041.

[45] K. Yasuda, J.M. Macak, S. Berger, A. Ghicov, P. Schmuki, Mechanistic aspects of the self-organization process for oxide nanotube formation on valve metals, J. Electrochem. Soc. 154 (2007) C472–C478, https://doi.org/10.1149/1.2749091.

[46] S. Kudelka, A. Michaelis, J. Schultze, Effect of texture and formation rate on ionic and electronic properties of passive layers on Ti single crystals, Electrochim. Acta 41 (1996) 863–870, https://doi.org/10.1016/0013-4686(95)00375-4.

[47] S. Kudelka, J.W. Schultze, Photoelectrochemical imaging and microscopic reactivity of oxidised Ti, Electrochim. Acta 42 (1997) 2817–2825, https://doi.org/10.1016/S0013-4686(97)00085-6.

[48] D. Khudhair, A. Bhatti, Y. Li, H.A. Hamedani, H. Garmestani, P. Hodgson, S. Nahavandi, Anodization parameters influencing the morphology and electrical properties of TiO_2 nanotubes for living cell interfacing and investigations, Mater. Sci. Eng. C 59 (2016) 1125–1142, https://doi.org/10.1016/j.msec.2015.10.042.

[49] M. Niinomi, Recent research and development in titanium alloys for biomedical applications and healthcare goods, Sci. Technol. Adv. Mater. 4 (2003) 445–454, https://doi.org/10.1016/j.stam.2003.09.002.

[50] T. Kokubo, H.-M. Kim, M. Kawashita, Novel bioactive materials with different mechanical properties, Biomaterials 24 (2003) 2161–2175, https://doi.org/10.1016/S0142-9612(03)00044-9.

[51] B.A. Sánchez-Escobedo, J.C. Escobedo-Bocardo, D.A. Cortés-Hernández, J.M. Almanza-Robles, G. García-Álvarez, Effect of the phosphorous content and synthesis method on the in vitro bioactivity and mechanical properties of calcium aluminate cements, Ceram. Int. 43 (2017) 13592–13601, https://doi.org/10.1016/j.ceramint.2017.07.068.

[52] J.M. Macak, H. Tsuchiya, P. Schmuki, High-aspect-ratio TiO_2 nanotubes by anodization of titanium, Angew. Chemie – Int. Ed. 44 (2005) 2100–2102, https://doi.org/10.1002/anie.200462459.

[53] J.A. Sorkin, S. Hughes, P. Soares, K.C. Popat, Titania nanotube arrays as interfaces for neural prostheses, Mater. Sci. Eng. C 49 (2015) 735–745, https://doi.org/10.1016/j.msec.2015.01.077.

[54] N.C. Verissimo, A. Cremasco, C.A. Rodrigues, R. Bertazzoli, R. Caram, In situ characterization of the effects of Nb and Sn on the anatase-rutile transition in TiO_2 nanotubes using high-temperature X-ray diffraction, Appl. Surf. Sci. 307 (2014) 372–381, https://doi.org/10.1016/j.apsusc.2014.04.040.

[55] J.M. Macak, H. Tsuchiya, A. Ghicov, K. Yasuda, R. Hahn, S. Bauer, P. Schmuki, TiO_2 nanotubes: self-organized electrochemical formation, properties and applications, Curr. Opin. Solid State Mater. Sci. 11 (2007) 3–18, https://doi.org/10.1016/j.cossms.2007.08.004.

[56] J.M. Chaves, A.L.A. Escada, A.D. Rodrigues, A.P.R. Alves Claro, Characterization of the structure, thermal stability and wettability of the TiO_2 nanotubes growth on the Ti-7.5Mo alloy surface, Appl. Surf. Sci. 370 (2016) 76–82, https://doi.org/10.1016/j.apsusc.2016.02.017.

[57] C. Nico, T. Monteiro, M.P.F. Graça, Niobium oxides and niobates physical properties: review and prospects, Prog. Mater. Sci. 80 (2016) 1–37, https://doi.org/10.1016/j.pmatsci.2016.02.001.

[58] D. Pradhan, A.W. Wren, S.T. Misture, N.P. Mellott, Investigating the structure and biocompatibility of niobium and titanium oxides as coatings for orthopedic metallic implants, Mater. Sci. Eng. C 58 (2016) 918–926, https://doi.org/10.1016/j.msec.2015.09.059.

[59] R. Kirchgeorg, W. Wei, K. Lee, S. So, P. Schmuki, Through-Hole, Self-Ordered Nanoporous Oxide Layers on Titanium, Niobium and Titanium-Niobium Alloys in Aqueous and Organic Nitrate Electrolytes, ChemistryOpen. 1 (2012) 21–25. http://doi.org/10.1002/open.201100012.

[60] A. Shivaram, S. Bose, A. Bandyopadhyay, Thermal degradation of TiO_2 nanotubes on titanium Anish, Appl. Surf. Sci. 317 (2014) 573–580, https://doi.org/10.1016/j.apsusc.2014.04.040.

[61] N.A. Dsouki, M.P. de Lima, R. Corazzini, T.M. Gáscon, L.A. Azzalis, V.B.C. ampos Junqueira, D. Feder, F.L.A. Fonseca, Cytotoxic, hematologic and histologic effects of niobium pentoxide in Swiss mice, J. Mater. Sci. Mater. Med. 25 (2014) 1301–1305. http://doi.org/10.1007/s10856-014-5153-0.

[62] D. Khudhair, H. Amani Hamedani, J. Gaburro, S. Shafei, S. Nahavandi, H. Garmestani, A. Bhatti, Enhancement of electro-chemical properties of TiO 2 nanotubes for biological interfacing, Mater. Sci. Eng. C 77 (2017) 111–120, https://doi.org/10.1016/j.msec.2017.03.112.

[63] Y.Q. Hao, S.J. Li, Y.L. Hao, Y.K. Zhao, H.J. Ai, Effect of nanotube diameters on bioactivity of a multifunctional titanium alloy, Appl. Surf. Sci. 268 (2013) 44–51, https://doi.org/10.1016/j.apsusc.2012.11.142.

[64] H.C. Hsu, S.C. Wu, S.K. Hsu, Y.C. Chang, W.F. Ho, Fabrication of nanotube arrays on commercially pure titanium and their apatite-forming ability in a simulated body fluid, Mater. Charact. 100 (2015) 170–177, https://doi.org/10.1016/j.matchar.2014.12.023.

[65] L. Yang, M. Zhang, S. Shi, J. Lv, S. Xueping, H. Gang, S. Zhaoqi, Effect of annealing temperature on wettability of TiO_2 nanotube array films, Nanoscale Res. Lett. 9 (2014) 621.

[66] A. Marmur, Wetting on Hydrophobic Rough Surfaces: To Be Heterogeneous or Not To Be?, Langmuir 19 (2003) 8343–8348, https://doiorg/10.1021/la0344682.

[67] K. Das, V.K. Balla, A. Bandyopadhyay, S. Bose, Surface modification of laser-processed porous titanium for load-bearing implants, Scr. Mater. 59 (2008) 822–825, https://doi.org/10.1016/j.scriptamat.2008.06.018.

[68] R.A. Gittens, L. Scheideler, F. Rupp, S.L. Hyzy, J. Geis-Gerstorfer, Z. Schwartz, B. D. Boyan, A review on the wettability of dental implant surfaces II: biological and clinical aspects, Acta Biomater. 10 (2014), https://doi.org/10.1016/j.actbio.2014.03.032.

[69] K.M. Hotchkiss, G.B. Reddy, S.L. Hyzy, Z. Schwartz, B.D. Boyan, R. Olivares-Navarrete, Titanium surface characteristics, including topography and wettability, alter macrophage activation, Acta Biomater. 31 (2016) 425–434, https://doi.org/10.1016/j.actbio.2015.12.003.